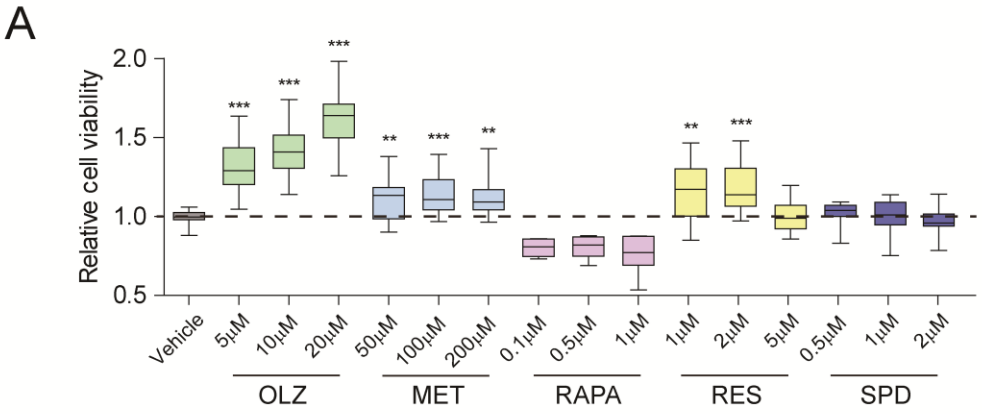
A
Relative cell viability
2.0
1.5
1.0
0.5
Vehicle
5μM
10μM
20μM
50μM
100μM
200μM
0.1μM
0.5μM
1μM
1μM
2μM
5μM
0.5μM
1μM
2μM
OLZ
MET
RAPA
RES
SPD

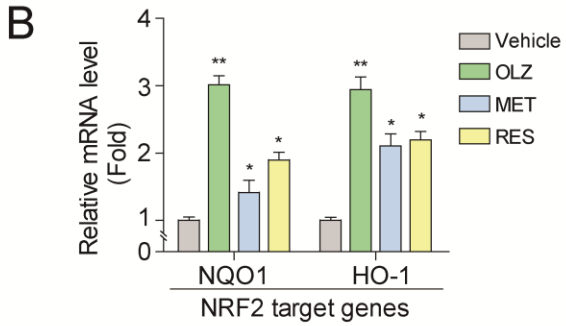
B
Relative mRNA level (Fold)
4
3
2
1
0
Vehicle
OLZ
MET
RES
NQO1
HO-1
NRF2 target genes

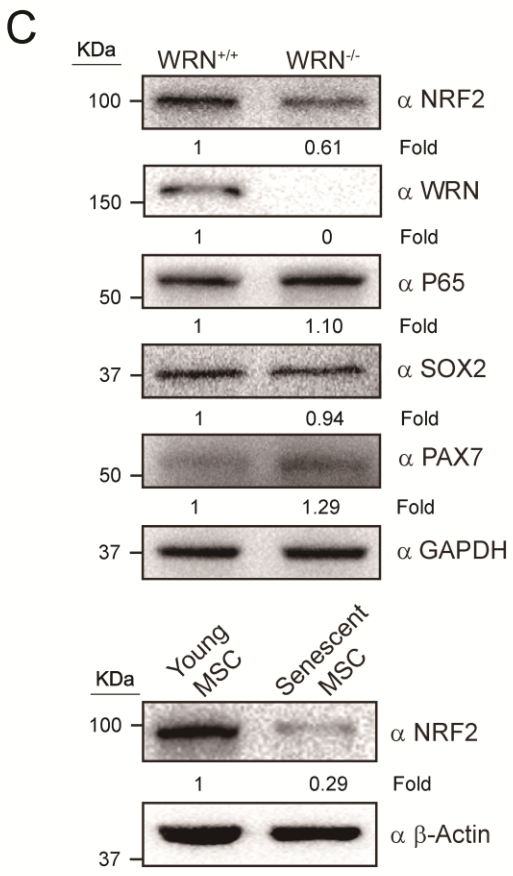
C
KDa
WRN+/+
WRN-/-
100
α NRF2
1
0.61
Fold
150
α WRN
1
0
Fold
50
α P65
1
1.10
Fold
37
α SOX2
1
0.94
Fold
50
α PAX7
1
1.29
Fold
37
α GAPDH
KDa
Young MSC
Senescent MSC
100
α NRF2
1
0.29
Fold
37
α β-Actin

Supplementary information, Figure S1. Gero-protective chemicals screen to identify candidates capable of alleviating senescence

(A) Clonally plated pre-senescent WS hMSCs (one passage prior to MSC senescence, P4) were treated with chemicals for over 2 weeks and cell viability was evaluated by MTS assay. Data were normalized to the vehicle control group (Vehicle). Plot was presented as Whiskers (Min to Max), n = 18, **P < 0.01, ***P < 0.001. Gero-protective chemicals were as follows: Oltipraz (OLZ), Metformin (MET), Rapamycin (RAPA), Resveratrol (RES) and Spermidine (SPD).

(B) RT-qPCR analysis of NRF2 target genes (*NQO1* and *HO-1*) in wild-type hMSCs (P2) with or without OLZ (10 μM), MET (100 μM) and RES (1 μM) treatments. Data were presented as mean ± SEM, n = 3, one-tail test, *P<0.05, **P < 0.01.

(C) Western blot analysis of NRF2 and other transcriptional factors in WS and in replicative senescent hMSCs. GAPDH and β-Actin were used as loading controls.

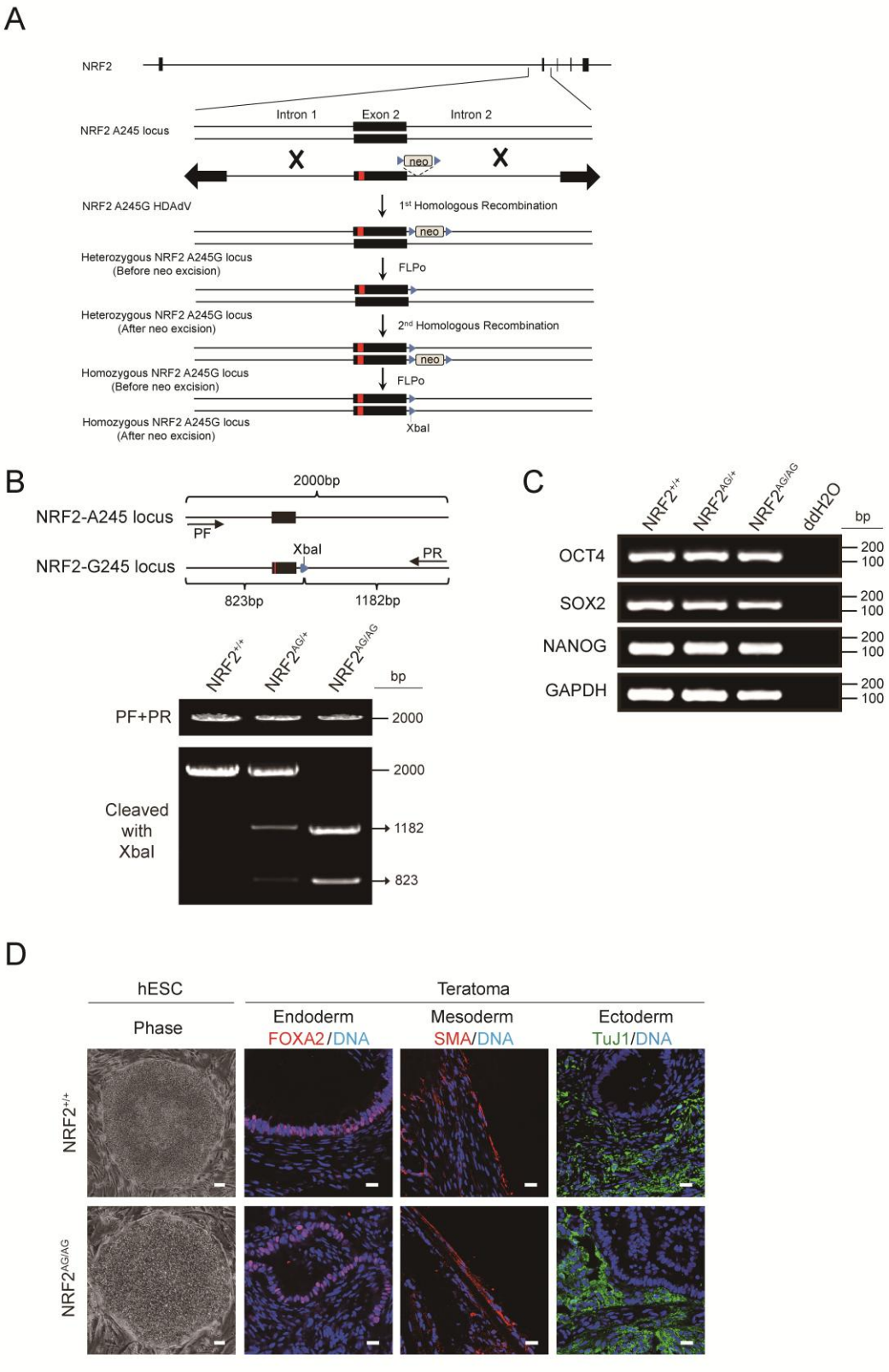
A
NRF2
Intron 1
Exon 2
Intron 2
NRF2 A245 locus
neo
NRF2 A245G HDAdV
1st Homologous Recombination
Heterozygous NRF2 A245G locus
(Before neo excision)
FLPo
Heterozygous NRF2 A245G locus
(After neo excision)
2nd Homologous Recombination
Homozygous NRF2 A245G locus
(Before neo excision)
FLPo
Homozygous NRF2 A245G locus
(After neo excision)
XbaI
B
2000bp
NRF2-A245 locus
PF
XbaI
PR
NRF2-G245 locus
823bp
1182bp
bp
PF+PR
2000
Cleaved with XbaI
1182
823
C
ddH2O
OCT4
SOX2
NANOG
GAPDH
200
100
D
hESC
Teratoma
Phase
Endoderm
FOXA2/DNA
Mesoderm
SMA/DNA
Ectoderm
TuJ1/DNA

Supplementary information, Figure S2. Generation of *NRF2*-A245G knock-in hESCs

(A) Schematic demonstration of *NRF2* gene editing strategy using *NRF2*-A245G-HDAdV. The point variation (A245G) in the *NRF2* locus results in a glutamic acid to glycine switch at amino acid 82 of the NRF2 protein and is supposed to lead to NRF2 stabilization and transcriptional activation of its target genes. Blue triangle, FRT site; Red stripe, A245G.

(B) Schematic diagram of restriction fragment length polymorphism (RFLP) identification in *NRF2*-A245 locus. Blue triangle, FRT site; Red stripe, A245G. Purified PCR products of *NRF2*-A245 locus in genomic DNAs of hESCs (top) were cleaved with XbaI (bottom) to verify successful homologous recombination.

(C) RT-PCR analysis of the pluripotency markers OCT4, SOX2, and NANOG in $NRF2^{+/+}$ and $NRF2^{AG/AG}$ hESCs. GAPDH, loading control.

(D) Representative bright-field (left) and immunofluorescence (right) images showing morphology of hESCs and expression of marker genes from the three germ layers in teratomas derived from hESCs, respectively. Scale bar, 100 μm (Phase), 20 μm (Ectoderm, Mesoderm and Endoderm).

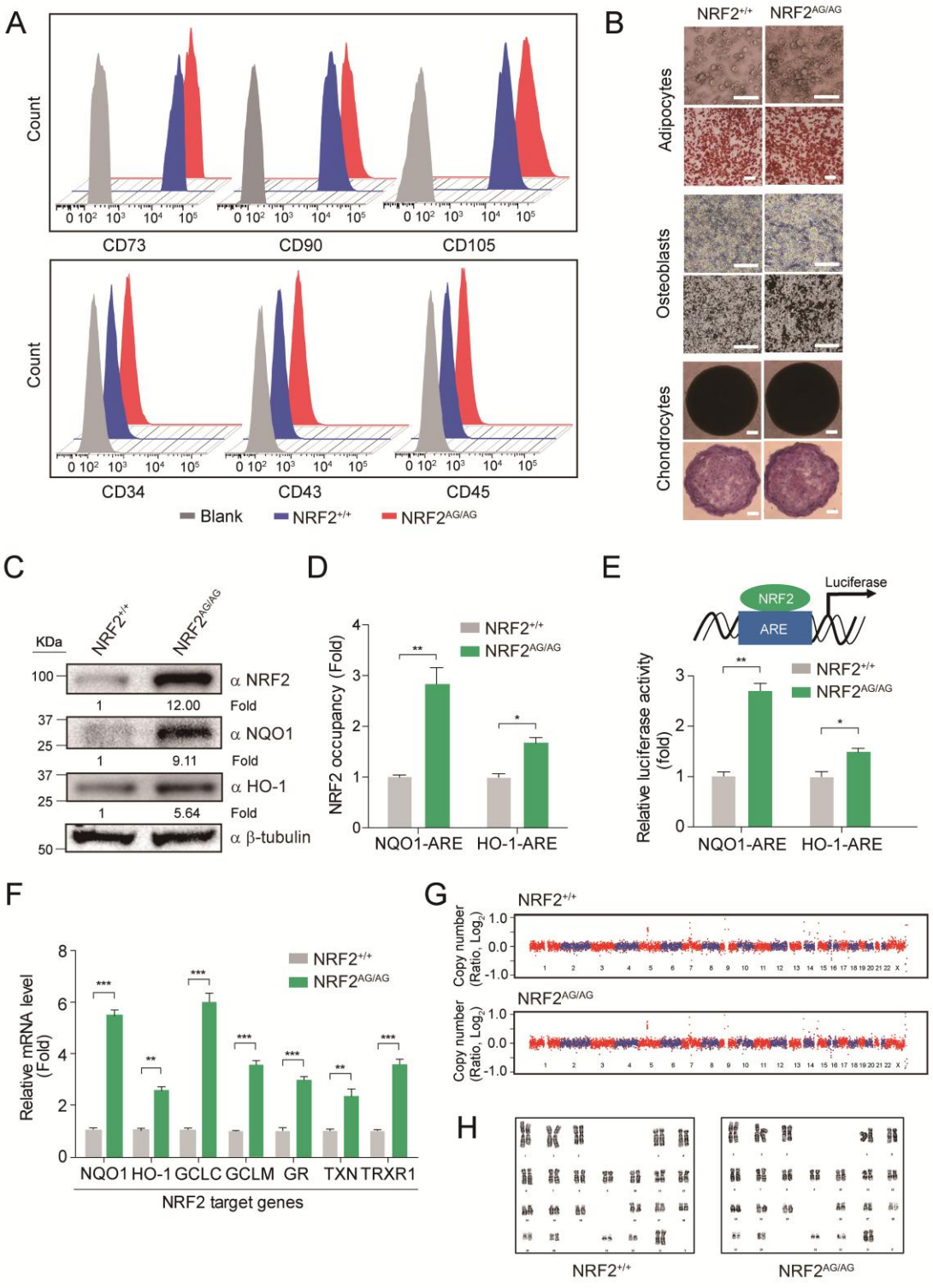
A
Count
CD73
CD90
CD105
CD34
CD43
CD45
Blank
NRF2+/+
NRF2AG/AG
B
NRF2+/+
NRF2AG/AG
Adipocytes
Osteoblasts
Chondrocytes
C
KDa
α NRF2
12.00
α NQO1
9.11
α HO-1
5.64
α β-tubulin
Fold
D
NRF2 occupancy (Fold)
NQO1-ARE
HO-1-ARE
E
Luciferase
NRF2
ARE
Relative luciferase activity (fold)
F
Relative mRNA level (Fold)
NQO1 HO-1 GCLC GCLM GR TXN TRXR1
NRF2 target genes
G
Copy number (Ratio, Log2)
H

Supplementary information, Figure S3. Characterization of *NRF2*$^{AG/AG}$ hMSC

(A) Flow cytometric analysis of MSC-specific surface markers (CD73, CD90 and CD105) and MSC-irrelevant markers (CD34, CD43 and CD45) in *NRF2*$^{+/+}$ and *NRF2*$^{AG/AG}$ hMSCs.

(B) Characterization of multiple-lineage differentiation potential of hMSCs. Oil Red O, Von Kossa and Toluidine blue O staining were used to evaluate adipogenesis, osteogenesis and chondrogenesis potential of MSCs, respectively. Bright field (upper); stained (lower). Scale bar, 100 μm.

(C) Western blot analysis of NRF2 and its target genes *NQO1* and *HO-1* in *NRF2*$^{+/+}$ and *NRF2*$^{AG/AG}$ hMSCs (P2). β-tubulin, loading control.

(D) ChIP-qPCR analysis of the enrichment of NRF2 at the cis-regulatory elements of *NQO1* and *HO-1* genes (NQO1-ARE and HO-1-ARE, respectively) in hMSCs (P2). Data were presented as mean ± SEM, n = 3, *P < 0.05, **P < 0.01.

(E) The transcriptional activity of endogenous NRF2 was measured by ARE-driven luciferase reporter assay. *NRF2*$^{+/+}$ and *NRF2*$^{AG/AG}$ hMSCs (P2) were co-transfected with NQO1/HO-1-ARE-luciferase and Renilla plasmids. Data were presented as mean ± SEM, n = 5, *P < 0.05, **P < 0.01.

(F) RT-qPCR analysis of NRF2 target genes in hMSCs (P2). Data were presented as mean ± SEM, n = 3, **P < 0.01, ***P < 0.001.

(G) Whole genome sequencing analysis of copy number variations (CNVs) in hMSCs (P5).

(H) G-banded karyotyping analysis of *NRF2*$^{+/+}$ and *NRF2*$^{AG/AG}$ hMSCs (P5).

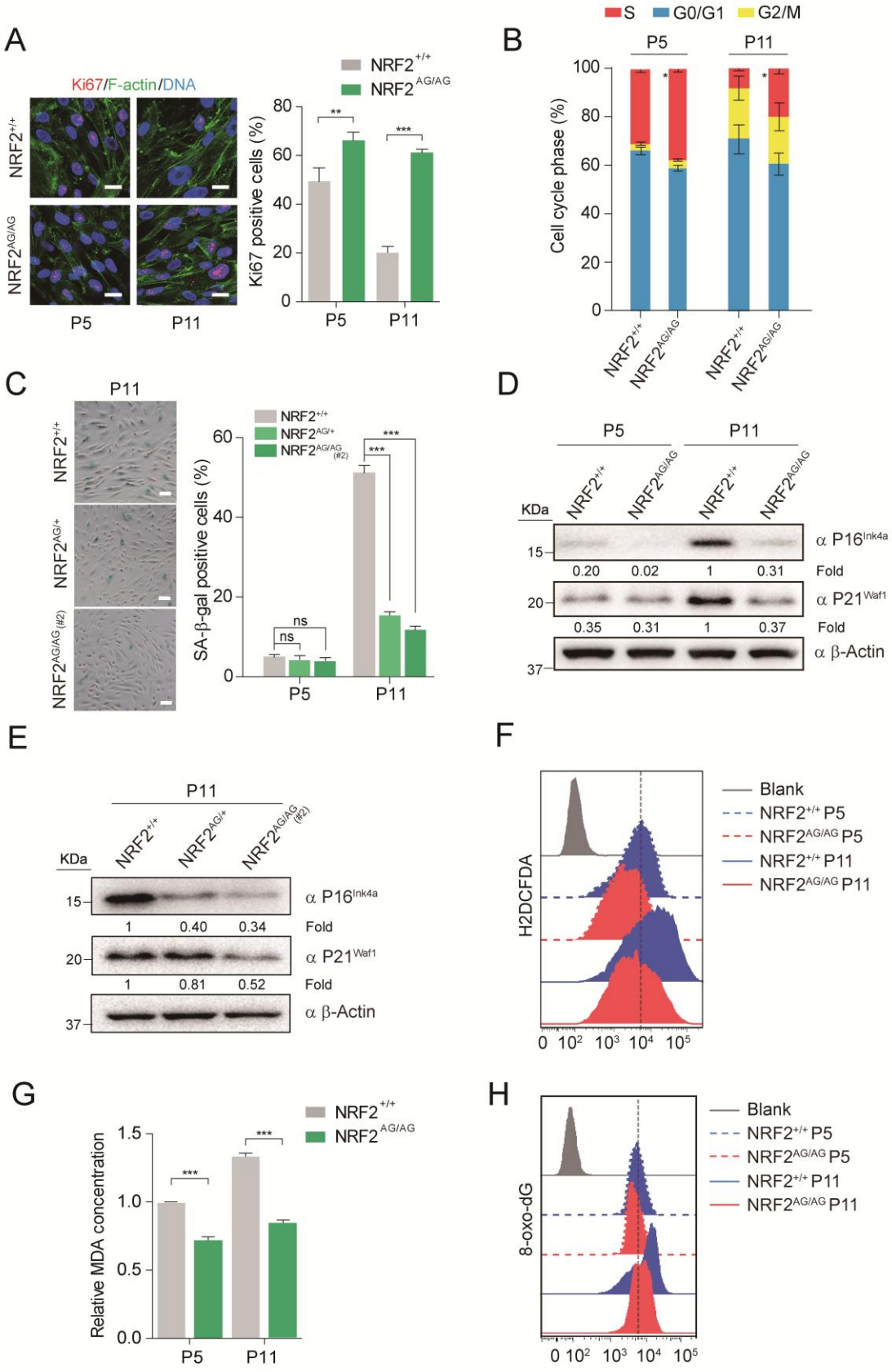
A
Ki67/F-actin/DNA
NRF2+/+
NRF2AG/AG
P5
P11
Ki67 positive cells (%)
B
S
G0/G1
G2/M
Cell cycle phase (%)
C
SA-β-gal positive cells (%)
ns
D
KDa
α P16Ink4a
α P21Waf1
α β-Actin
Fold
E
F
Blank
H2DCFDA
G
Relative MDA concentration
H
8-oxo-dG

Supplementary information, Figure S4. Activating the NRF2 pathway confers cellular senescence- resistance to cultured hMSCs

(A-B) *NRF2*$^{AG/AG}$ hMSCs maintained a cell cycle profile characteristic of proliferating cells from P5 to P11. (A) Ki67 immunostaining analysis of *NRF2*$^{+/+}$ and *NRF2*$^{AG/AG}$ hMSCs at P5 and P11. Scale bar, 20 μm. Data were presented as mean ± SEM, n = 6, **P < 0.01, ***P < 0.001. (B) Cell cycle analysis of *NRF2*$^{+/+}$ and *NRF2*$^{AG/AG}$ hMSCs at P5 and P11. Data were presented as Mean ± SEM, n = 3, Statistical significance of cell percentage in S phase were compared between *NRF2*$^{+/+}$ and *NRF2*$^{AG/AG}$ hMSCs, *P < 0.05.

(C) SA-β-gal staining of *NRF2*$^{+/+}$, *NRF2*$^{AG/+}$ and *NRF2*$^{AG/AG}{}_{(\#2)}$ hMSCs at P5 and P11. Scale bar, 50 μm. Data were presented as mean ± SEM, n = 8, ns: not significant, ***P < 0.001.

(D) Western blot analysis of P16^{Ink4a} and P21^{waf1} proteins in P5 and P11 hMSCs. β-Actin, loading control.

(E)Western blot analysis of aging-associated P16^{Ink4a} and P21^{waf1} protein in *NRF2*$^{+/+}$, *NRF2*$^{AG/+}$ and *NRF2*$^{AG/AG}{}_{(\#2)}$ hMSCs (P11). β-Actin, loading control.

(F) Detection of cellular reactive oxygen species (ROS) levels in hMSCs with H2DCFDA probes.

(G) Detection of a lipid oxidation product malondialdehyde (MDA) in *NRF2*$^{+/+}$ and *NRF2*$^{AG/AG}$ hMSCs at P5 and P11. Data were normalized to cell numbers, n = 3, ***P < 0.001.

(H) Flow cytometric analysis of DNA oxidation indicator 8-oxo-7, 8-dihydro-2'-deoxyguanosine (8-oxo-dG) levels in hMSCs at P5 and P11.

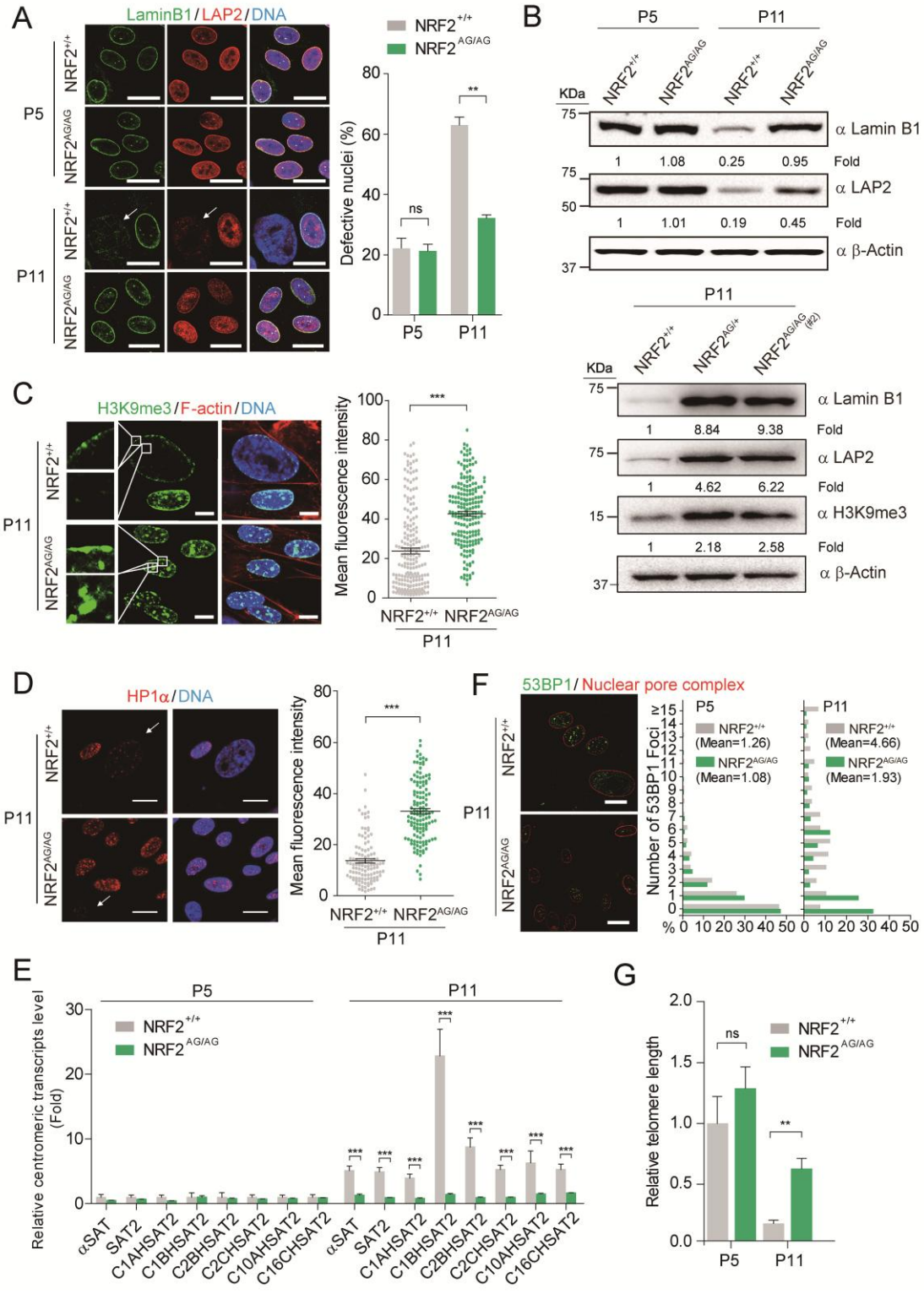
A
LaminB1 / LAP2 / DNA
P5
P11
NRF2+/+
NRF2AG/AG
Defective nuclei (%)
ns
**
B
P5
P11
KDa
α Lamin B1
α LAP2
α β-Actin
Fold
P11
NRF2AG/+
NRF2AG/AG (#2)
C
H3K9me3 / F-actin / DNA
Mean fluorescence intensity
***
D
HP1α / DNA
E
Relative centromeric transcripts level (Fold)
αSAT
SAT2
C1AHSAT2
C1BHSAT2
C2BHSAT2
C2CHSAT2
C10AHSAT2
C16CHSAT2
F
53BP1 / Nuclear pore complex
Number of 53BP1 Foci
(Mean=1.26)
(Mean=1.08)
(Mean=4.66)
(Mean=1.93)
G
Relative telomere length

Supplementary information, Figure S5. *NRF2*$^{AG/AG}$ hMSCs repressed senescence-associated defects in nuclear envelope and (epi-)genome

(A-B) *NRF2*$^{AG/AG}$ hMSCs were resistant to aging-associated NE defects. (A) Immunofluorescence analysis of Lamin B1 and LAP2 expression in hMSCs. White arrows denote the nuclear envelope-defective cells with decreased Lamin B1 and LAP2 expression. Scale bar, 20 μm. Data were presented as mean ± SEM, n = 8, ns: not significant, ***P < 0.001. (B) Western blot analysis of Lamin B1 and LAP2 protein in hMSCs. β-Actin, loading control.

(C-E) *NRF2*$^{AG/AG}$ hMSCs were resistant to aging-associated epigenetic alteration. Representative immunofluorescence images of heterochromatin marks H3K9me3 (C) and HP1α (D) in *NRF2*$^{+/+}$ and *NRF2*$^{AG/AG}$ hMSCs at P11. Scale bar, 10 μm. White arrows denote cells with decreased HP1α expression. Mean fluorescence intensities of H3K9m3 and HP1α were measured by ImageJ. Data were presented as mean ± SEM. >100 nuclei from 10 images were scored, ***P < 0.001. (E) RT-qPCR analysis of the centromeric satellite DNA transcripts in *NRF2*$^{+/+}$ and *NRF2*$^{AG/AG}$ hMSCs. Consistent with the loss of heterochromatin marks, the overrepresentation of transcripts from centromeric satellite DNA normally seen in *NRF2*$^{+/+}$ hMSCs undergoing replicative senescence was not observed in *NRF2*$^{AG/AG}$ hMSCs at P11. Data were presented as mean ± SEM, n=3, ***P < 0.001.

(F-G) *NRF2*$^{AG/AG}$ hMSCs were resistant to aging-associated accumulation of genome damage. (F) The number of 53BP1 foci per nucleus in the nuclei of *NRF2*$^{+/+}$ and *NRF2*$^{AG/AG}$ hMSCs at P5 and P11 was quantified. *NRF2*$^{AG/AG}$ hMSCs exhibited less accumulation of nuclear 53BP1 foci. >200 nuclei from 10 images were scored. Scale bar, 20 μm. (G) Quantitative RT-PCR analysis of relative telomere length showing milder telomere attrition in *NRF2*$^{AG/AG}$ hMSCs. Data were normalized to the value of P5 *NRF2*$^{+/+}$ group and presented as mean ± SEM, n=5, ns: not significant, **P < 0.01.

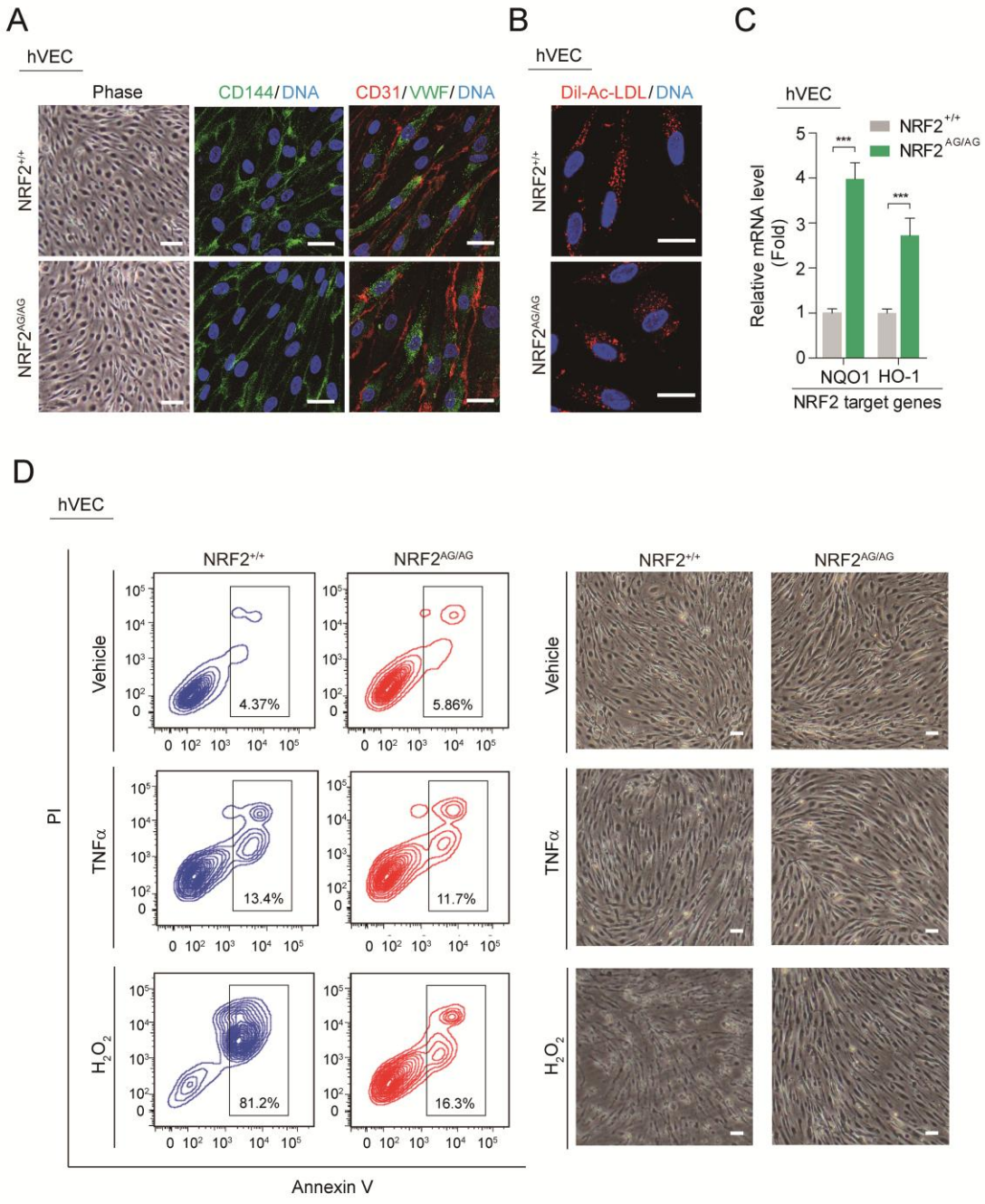
A
hVEC
Phase
CD144/DNA
CD31/VWF/DNA
NRF2+/+
NRF2AG/AG
B
hVEC
Dil-Ac-LDL/DNA
NRF2+/+
NRF2AG/AG
C
hVEC
NRF2+/+
NRF2AG/AG
Relative mRNA level (Fold)
***
***
NQO1
HO-1
NRF2 target genes
D
hVEC
NRF2+/+
NRF2AG/AG
Vehicle
TNFα
H2O2
PI
Annexin V
4.37%
5.86%
13.4%
11.7%
81.2%
16.3%

Supplementary information, Figure S6. *NRF2*$^{AG/AG}$ hVECs exhibited resistance to oxidative stress

(A) Representative bright-field (left) and immunofluorescence (right) images showing morphology of hVECs and expression of endothelial cell-specific markers CD144, CD31 and VWF in *NRF2*$^{+/+}$ and *NRF2*$^{AG/AG}$ hVECs. Scale bar, 200 μm (Phase), 50 μm (immunofluorescence images).

(B) The uptake of Dil-Ac-LDL (dioctadecylindocarbocyanine-labeled acetylated low-density lipoprotein) in *NRF2*$^{+/+}$ and *NRF2*$^{AG/AG}$ hVECs. Scale bar, 25 μm.

(C) RT-qPCR analysis confirmed that the NRF2 was activated in *NRF2*$^{AG/AG}$ hVECs. Data were presented as mean ± SEM, n = 3, ***P < 0.001.

(D) *NRF2*$^{+/+}$ and *NRF2*$^{AG/AG}$ hVECs were treated with 10 ng/mL TNFα or 500 μM H_2O_2 for 24 h, and the apoptotic cells were determined by Annexin V-PI staining via flow cytometric analysis. Specifically, *NRF2*$^{AG/AG}$ hVECs exhibited resistance to H_2O_2-induced apoptosis.

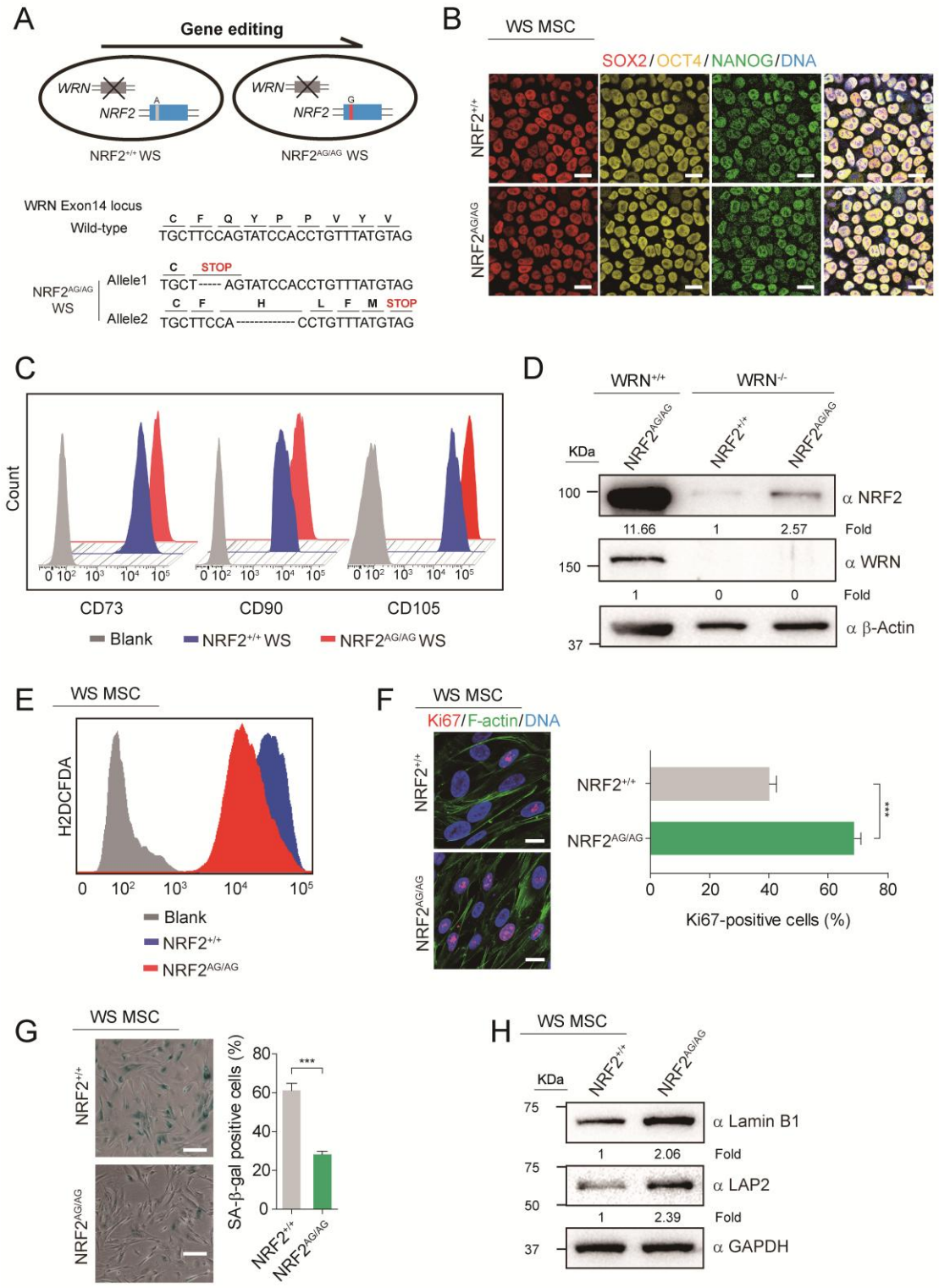
A
Gene editing
WRN
NRF2
A
G
NRF2+/+ WS
NRF2AG/AG WS
WRN Exon14 locus
Wild-type
C F Q Y P P V Y V
TGCTTCCAGTATCCACCTGTTTATGTAG
NRF2AG/AG WS
Allele1
C STOP
TGCT----- AGTATCCACCTGTTTATGTAG
Allele2
C F H L F M STOP
TGCTTCCA---------- CCTGTTTATGTAG
B
WS MSC
SOX2/OCT4/NANOG/DNA
NRF2+/+
NRF2AG/AG
C
Count
CD73
CD90
CD105
Blank
NRF2+/+ WS
NRF2AG/AG WS
D
WRN+/+
WRN-/-
KDa
NRF2AG/AG
NRF2+/+
NRF2AG/AG
100
α NRF2
11.66
1
2.57
Fold
150
α WRN
1
0
0
Fold
37
α β-Actin
E
WS MSC
H2DCFDA
Blank
NRF2+/+
NRF2AG/AG
F
WS MSC
Ki67/F-actin/DNA
NRF2+/+
NRF2AG/AG
NRF2+/+
NRF2AG/AG
***
Ki67-positive cells (%)
G
WS MSC
NRF2+/+
NRF2AG/AG
SA-β-gal positive cells (%)
***
H
WS MSC
KDa
NRF2+/+
NRF2AG/AG
75
α Lamin B1
1
2.06
Fold
75
50
α LAP2
1
2.39
Fold
37
α GAPDH

Supplementary information, Figure S7. Genetic modification of *NRF2* relieved the premature senescence in a WS background

(A) Schematic diagram showing the strategy of genetic modification in hESCs to generate the *NRF2*-A245G knock-in WS hESCs. Genotyping result was shown at the bottom.

(B) Immunofluorescence analysis of pluripotency marker gene expressions in $NRF2^{+/+}$ and $NRF2^{AG/AG}$ WS hESCs. Scale bar, 20 μm.

(C) Flow cytometric analysis of MSC-specific surface markers CD73, CD90, and CD105 in $NRF2^{+/+}$ and $NRF2^{AG/AG}$ WS hMSCs.

(D) Western blot analysis of NRF2 and WRN proteins in $NRF2^{+/+}$ and $NRF2^{AG/AG}$ WS hMSCs. β-Actin, loading control.

(E) Constitutive activation of NRF2 repressed ROS contents in $NRF2^{AG/AG}$ WS hMSCs.

(F-H) Genetic enhancement of NRF2 in WS hMSCs alleviated accelerated aging phenotypes (i.e., reduced proliferation capacity, increase in SA-β-gal positive cells, and diminished expression of nuclear envelope-associated proteins). (F) Ki67 immunostaining analysis of $NRF2^{+/+}$ and $NRF2^{AG/AG}$ WS hMSCs. Scale bar, 20 μm. Data were presented as mean ± SEM, n = 6, ***P < 0.001. (G) SA-β-gal staining of $NRF2^{+/+}$ and $NRF2^{AG/AG}$ WS hMSCs. Scale bar, 50 μm. Data were presented as mean ± SEM, n = 6, ***P < 0.001. (H) Western blot analysis of Lamin B1 and LAP2 proteins in $NRF2^{+/+}$ and $NRF2^{AG/AG}$ WS hMSCs. GAPDH, loading control.

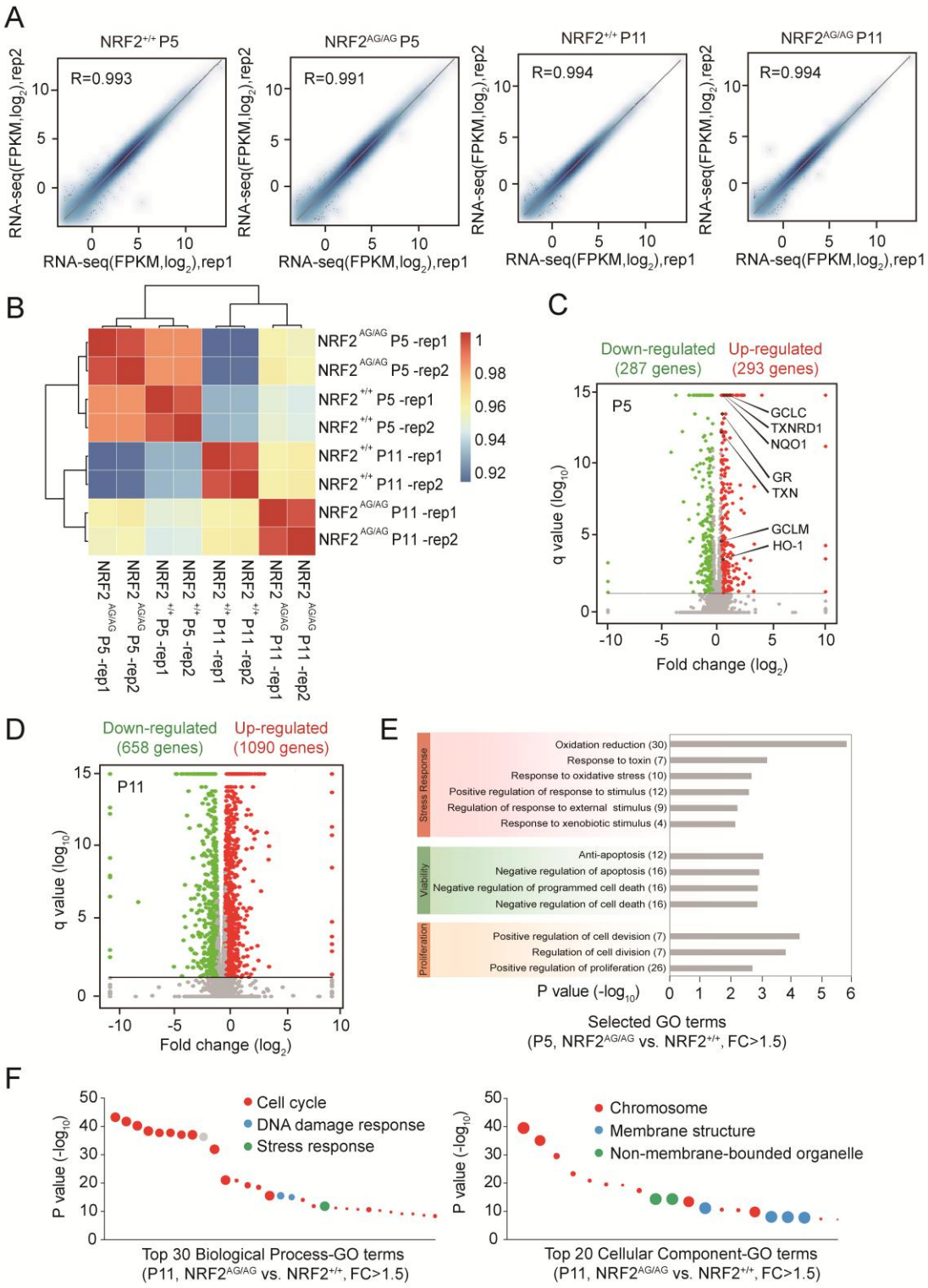
A
NRF2+/+ P5
R=0.993
NRF2AG/AG P5
R=0.991
NRF2+/+ P11
R=0.994
NRF2AG/AG P11
R=0.994
RNA-seq(FPKM,log2),rep2
RNA-seq(FPKM,log2),rep1
B
NRF2 AG/AG P5 -rep1
NRF2 AG/AG P5 -rep2
NRF2 +/+ P5 -rep1
NRF2 +/+ P5 -rep2
NRF2 +/+ P11 -rep1
NRF2 +/+ P11 -rep2
NRF2 AG/AG P11 -rep1
NRF2 AG/AG P11 -rep2
1
0.98
0.96
0.94
0.92
C
Down-regulated (287 genes)
Up-regulated (293 genes)
P5
GCLC
TXNRD1
NQO1
GR
TXN
GCLM
HO-1
q value (log10)
Fold change (log2)
D
Down-regulated (658 genes)
Up-regulated (1090 genes)
P11
q value (log10)
Fold change (log2)
E
Stress Response
Oxidation reduction (30)
Response to toxin (7)
Response to oxidative stress (10)
Positive regulation of response to stimulus (12)
Regulation of response to external stimulus (9)
Response to xenobiotic stimulus (4)
Viability
Anti-apoptosis (12)
Negative regulation of apoptosis (16)
Negative regulation of programmed cell death (16)
Negative regulation of cell death (16)
Proliferation
Positive regulation of cell devision (7)
Regulation of cell division (7)
Positive regulation of proliferation (26)
P value (-log10)
Selected GO terms
(P5, NRF2AG/AG vs. NRF2+/+, FC>1.5)
F
Cell cycle
DNA damage response
Stress response
P value (-log10)
Top 30 Biological Process-GO terms
(P11, NRF2AG/AG vs. NRF2+/+, FC>1.5)
Chromosome
Membrane structure
Non-membrane-bounded organelle
Top 20 Cellular Component-GO terms
(P11, NRF2AG/AG vs. NRF2+/+, FC>1.5)

Supplementary information, Figure S8. Global gene expression analysis of P5 and P11 hMSCs

(A) Scatter plots showing the correlation of gene expression (FPKM > 0.1) between duplicates of P5 and P11 *NRF2*$^{+/+}$ and *NRF2*$^{AG/AG}$ hMSCs, respectively. The Spearman correlation coefficient was shown at the left upper side of each panel.

(B) Heatmap showing correlation of gene expression between 8 hMSC samples.

(C) Volcano plot showing differentially expressed genes (*NRF2*$^{+/+}$ vs. *NRF2*$^{AG/AG}$ <0.67, *NRF2*$^{+/+}$ vs. *NRF2*$^{AG/AG}$ >1.5, q< 0.05) between *NRF2*$^{+/+}$ and *NRF2*$^{AG/AG}$ hMSCs at P5. Representative NRF2 target genes were highlighted.

(D) Volcano plot showing differentially expressed genes (*NRF2*$^{+/+}$ vs. *NRF2*$^{AG/AG}$ <0.67, *NRF2*$^{+/+}$ vs. *NRF2*$^{AG/AG}$ >1.5, q< 0.05) between *NRF2*$^{+/+}$ and *NRF2*$^{AG/AG}$ hMSCs at P11.

(E) Selected GO term enrichment for the upregulated genes (*NRF2*$^{AG/AG}$ vs. *NRF2*$^{+/+}$ >1.5, q< 0.05) in P5 hMSCs, FC: fold change. The number of genes included in each category was shown in brackets after the term name and P ($-\log_{10}$) values were indicated by grey columns.

(F) Top 30 biological processes and 20 cellular component GO terms enriched in the up-regulated genes in P11 hMSCs, FC: fold change. The number of genes included in each terms was indicated by the size of point.

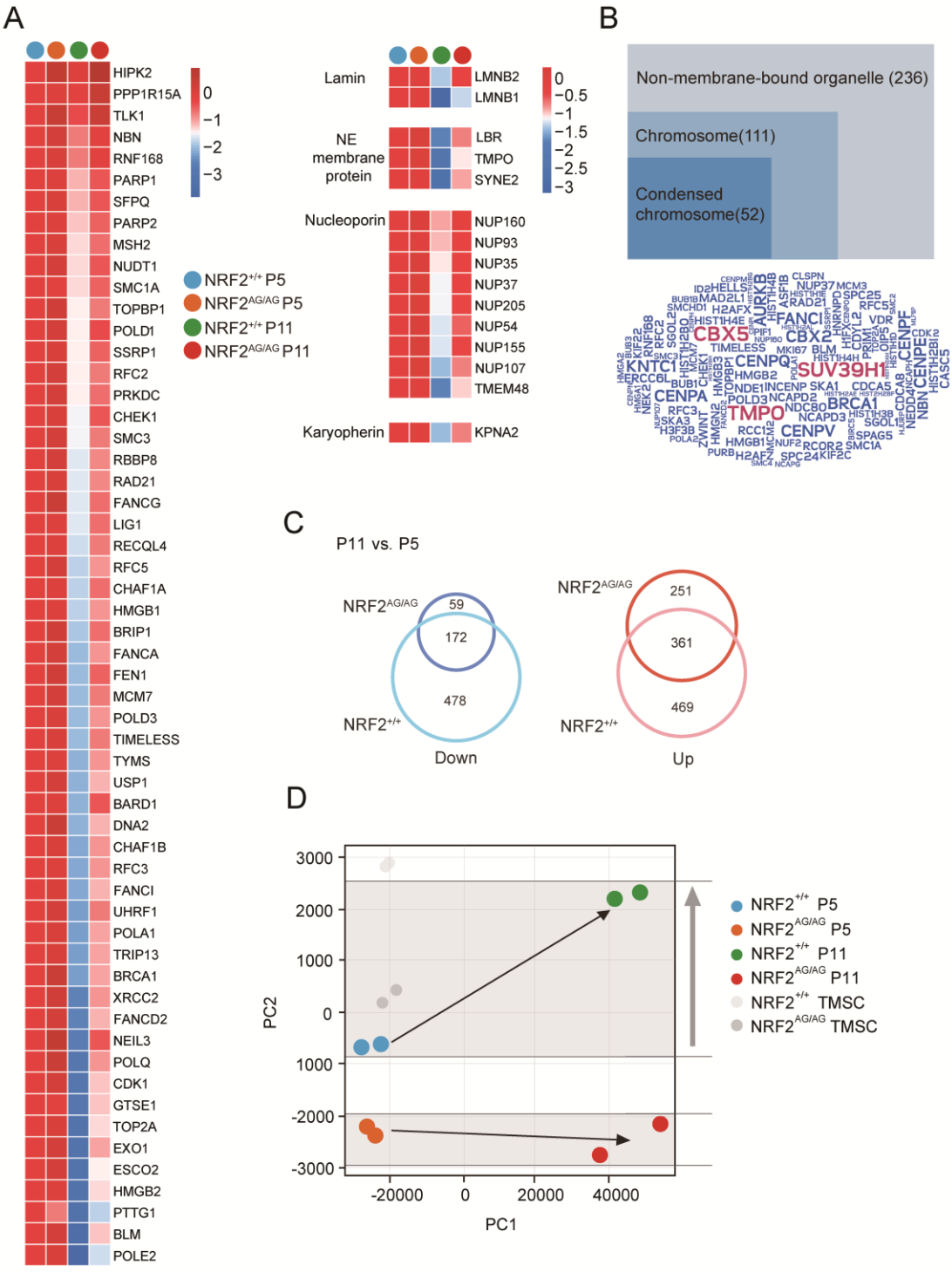
A
HIPK2
PPP1R15A
TLK1
NBN
RNF168
PARP1
SFPQ
PARP2
MSH2
NUDT1
SMC1A
TOPBP1
POLD1
SSRP1
RFC2
PRKDC
CHEK1
SMC3
RBBP8
RAD21
FANCG
LIG1
RECQL4
RFC5
CHAF1A
HMGB1
BRIP1
FANCA
FEN1
MCM7
POLD3
TIMELESS
TYMS
USP1
BARD1
DNA2
CHAF1B
RFC3
FANCI
UHRF1
POLA1
TRIP13
BRCA1
XRCC2
FANCD2
NEIL3
POLQ
CDK1
GTSE1
TOP2A
EXO1
ESCO2
HMGB2
PTTG1
BLM
POLE2
0
−1
−2
−3
Lamin
LMNB2
LMNB1
NE membrane protein
LBR
TMPO
SYNE2
Nucleoporin
NUP160
NUP93
NUP35
NUP37
NUP205
NUP54
NUP155
NUP107
TMEM48
Karyopherin
KPNA2
0
−0.5
−1
−1.5
−2
−2.5
−3
NRF2+/+ P5
NRF2AG/AG P5
NRF2+/+ P11
NRF2AG/AG P11
B
Non-membrane-bound organelle (236)
Chromosome(111)
Condensed chromosome(52)
C
P11 vs. P5
NRF2AG/AG
59
172
478
NRF2+/+
Down
NRF2AG/AG
251
361
469
NRF2+/+
Up
D
3000
2000
1000
0
1000
-2000
-3000
PC2
-20000
0
20000
40000
PC1
NRF2+/+ P5
NRF2AG/AG P5
NRF2+/+ P11
NRF2AG/AG P11
NRF2+/+ TMSC
NRF2AG/AG TMSC

Supplementary information, Figure S9. A rejuvenated cellular state revealed by gene expression profile of *NRF2*$^{AG/AG}$ hMSCs

(A) Heatmap showing the expression levels of the DNA damage response (left) and nuclear envelope (right) -associated genes were maintained in P11 *NRF2*$^{AG/AG}$ hMSCs. All FPKMs of the indicated genes were normalized by the ones in P5 *NRF2*$^{+/+}$ group and the relative expression level were presented as Log_2 (Ratio).

(B) Selected chromosome organization-associated GO terms for upregulated genes in P11 hMSCs (*NRF2*$^{AG/AG}$ vs. *NRF2*$^{+/+}$ >1.5, q< 0.05). The number of genes included in each category was shown in brackets after the term name. Lower word cloud showing all 111 up-regulated chromosome organization-associated genes. Senescence-associated heterochromatin organizers SUV39H1, CBX5 (HP1α) and TMPO (LAP2) were highlighted.

(C) Venn diagram showing the numbers of the upregulated genes and downregulated genes during serial passaging (P11 vs. P5) of *NRF2*$^{+/+}$ and *NRF2*$^{AG/AG}$ hMSCs. In *NRF2*$^{+/+}$ hMSCs, the altered genes were identified as "signatures of replicative senescence", which included 650 down-regulated genes and 831 up-regulated genes (FC >2 or FC <0.5). In comparison, less pronounced transcriptional changes were observed in *NRF2*$^{AG/AG}$ hMSCs, with only 231 down-regulated genes and 613 up-regulated genes.

(D) Principal component analysis (PCA) of RNA-Seq data of P5 and P11 *NRF2*$^{+/+}$ and *NRF2*$^{AG/AG}$ hMSCs using genes with FPKM > 0.1.

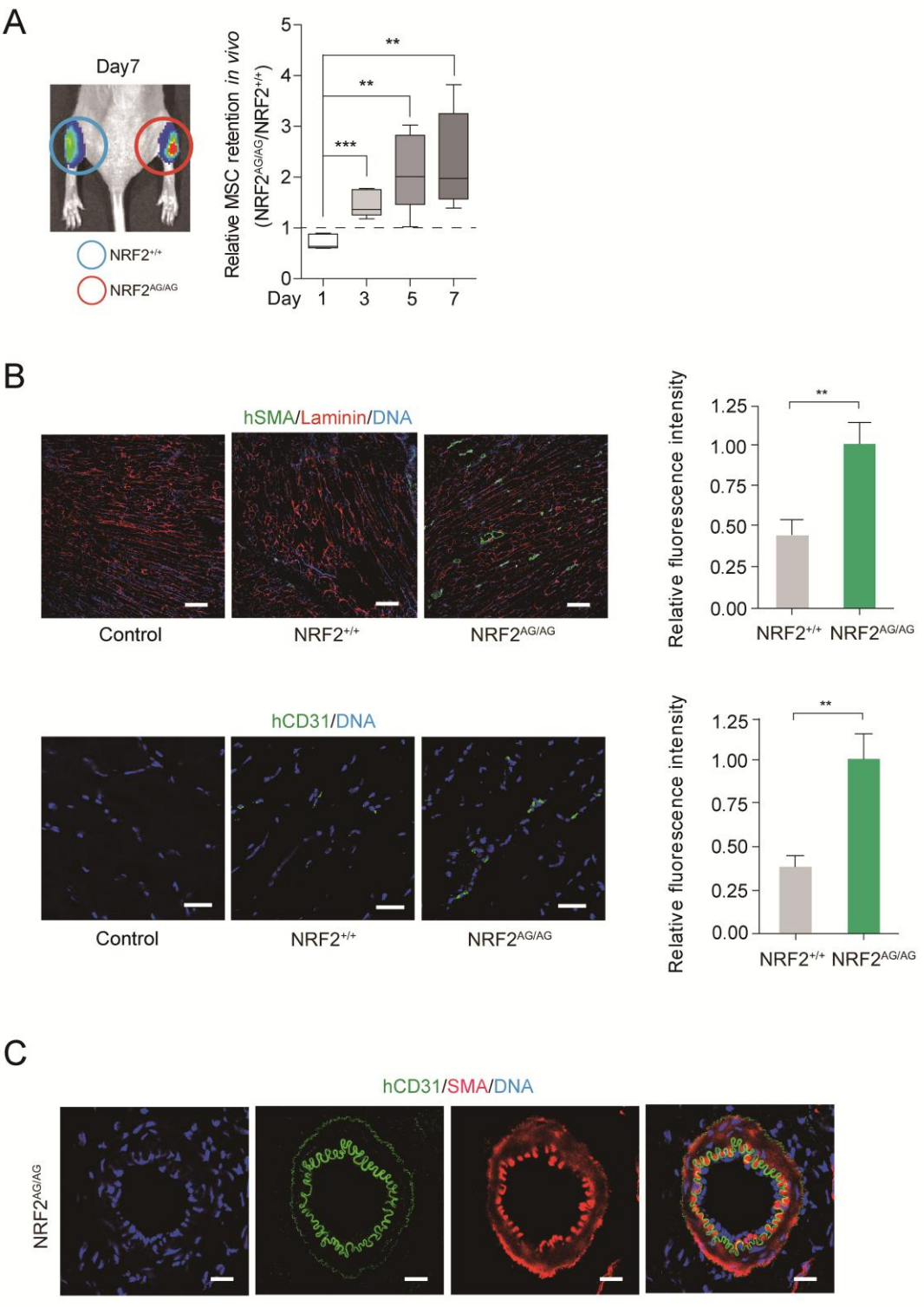
A
Day7
NRF2+/+
NRF2AG/AG
Relative MSC retention in vivo
(NRF2AG/AG/NRF2+/+)
Day 1 3 5 7
B
hSMA/Laminin/DNA
Control
NRF2+/+
NRF2AG/AG
Relative fluorescence intensity
NRF2+/+ NRF2AG/AG
hCD31/DNA
Control
NRF2+/+
NRF2AG/AG
Relative fluorescence intensity
NRF2+/+ NRF2AG/AG
C
hCD31/SMA/DNA
NRF2AG/AG

Supplementary information, Figure S10. *In vivo* survival and conversion of transplanted hMSCs to vascular-related cells in a mouse hindlimb ischemia model

(A) Photon flux from TA muscle of nude mice transplanted with luciferase-labeled *NRF2*$^{+/+}$ (left) and *NRF2*$^{AG/AG}$ (right) hMSCs (P8). Data were presented as relative luminescent signals (*NRF2*$^{AG/AG}$ vs. *NRF2*$^{+/+}$) and plot was presented as Whiskers (Min to Max), n=5, **P < 0.01, ***P < 0.001.

(B) Representative immunofluorescence images showing the presence of hCD31 and hSMA-positive human cells in the muscle tissue of hindlimb ischemic mice 4 weeks after hMSC transplantation. Scale bar, 200 μm (hSMA) and 50 μm (hCD31), respectively. Mean fluorescence intensity from 6 images were determined by ImageJ. Data were normalized to the *NRF2*$^{AG/AG}$ hMSC group and presented as mean ± SEM, n = 6, **P < 0.01.

(C) Representative immunofluorescence images showing neovascularization in ischemic hindlimb receiving *NRF2*$^{AG/AG}$ hMSCs. Scale bar, 20 μm.

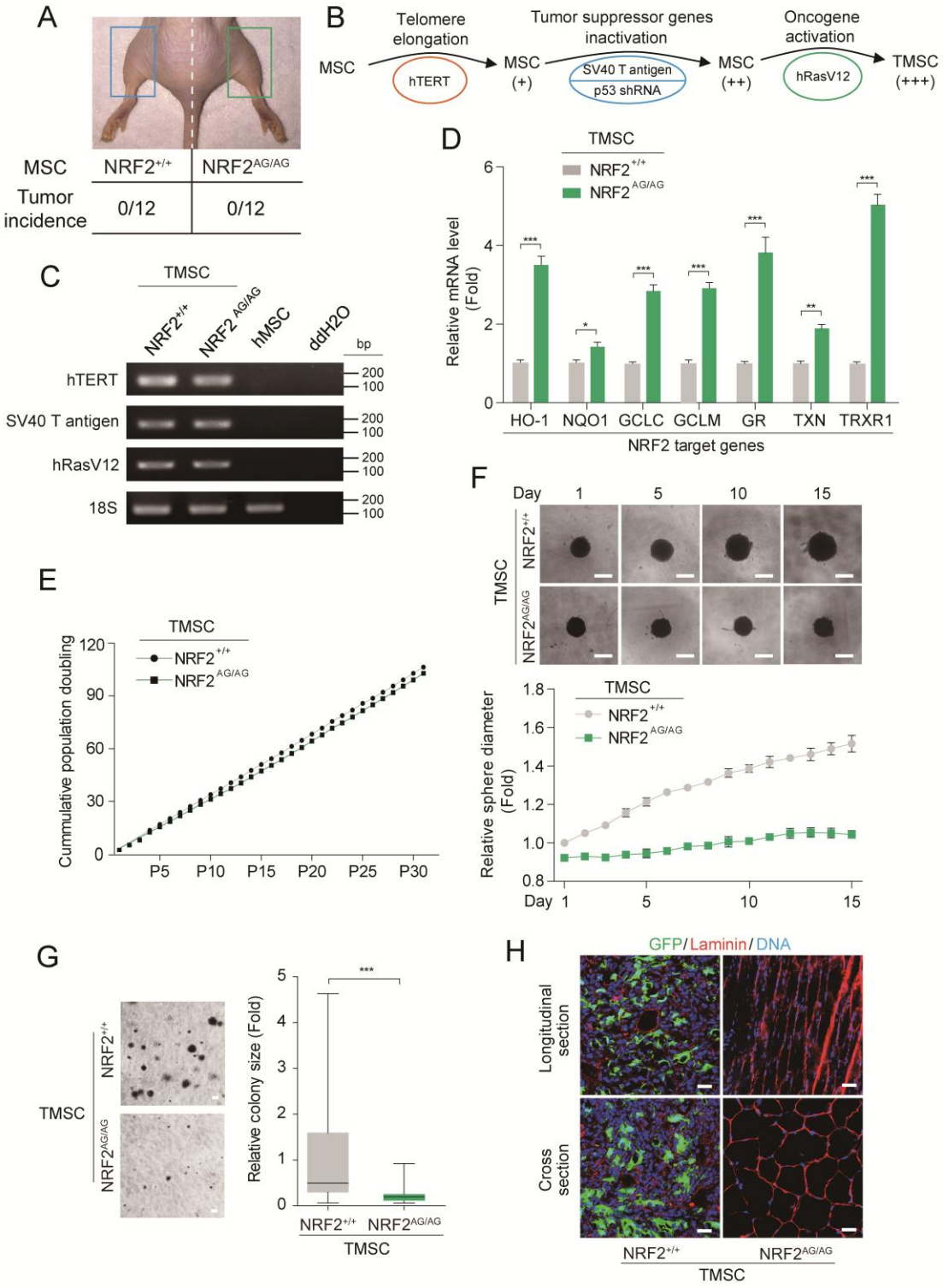
A
MSC
NRF2+/+
NRF2AG/AG
Tumor incidence
0/12
0/12
B
MSC
Telomere elongation
hTERT
MSC (+)
Tumor suppressor genes inactivation
SV40 T antigen
p53 shRNA
MSC (++)
Oncogene activation
hRasV12
TMSC (+++)
C
TMSC
NRF2+/+
NRF2 AG/AG
hMSC
ddH2O
bp
hTERT
SV40 T antigen
hRasV12
18S
200
100
D
TMSC
NRF2+/+
NRF2 AG/AG
Relative mRNA level (Fold)
HO-1
NQO1
GCLC
GCLM
GR
TXN
TRXR1
NRF2 target genes
E
TMSC
NRF2+/+
NRF2 AG/AG
Cummulative population doubling
P5
P10
P15
P20
P25
P30
F
Day
1
5
10
15
TMSC
NRF2+/+
NRF2AG/AG
TMSC
NRF2+/+
NRF2 AG/AG
Relative sphere diameter (Fold)
Day
G
TMSC
NRF2+/+
NRF2AG/AG
Relative colony size (Fold)
NRF2+/+
NRF2AG/AG
TMSC
H
GFP/Laminin/DNA
Longitudinal section
Cross section
NRF2+/+
NRF2AG/AG
TMSC

Supplementary information, Figure S11. *NRF2*$^{AG/AG}$ hMSCs display resistance to oncogenes-induced neoplastic transformation

(A) A representative image showing long-term *in vivo* consequences after hMSCs (P5) transplantation. Images and tumor incidence were obtained 6 months after transplantation.

(B) Schematic representation of transforming hMSCs into TMSCs via an *in vitro* oncogenic transformation procedure. This *in vitro* transformation system encompasses different sequential molecular events, which include elongation of telomeres, perturbation of the tumor suppressors p53 and pRb, as well as overexpression of oncogenic Ras^{G12V} protein.

(C) RT-PCR analysis of the indicated oncogenic transformation factors showing these factors were expressed at comparable levels in *NRF2*$^{+/+}$ and *NRF2*$^{AG/AG}$ TMSCs. Untransformed WT hMSCs were used as a negative control.

(D) RT-qPCR analysis confirmed that the NRF2 pathway was constitutively activated in *NRF2*$^{AG/AG}$ TMSCs. Data were presented as mean ± SEM, n = 3, *P < 0.05, **P < 0.01, ***P < 0.001.

(E) Growth curve showing the accumulative population doubling of *NRF2*$^{+/+}$ and *NRF2*$^{AG/AG}$ TMSCs. Both *NRF2*$^{+/+}$and *NRF2*$^{AG/AG}$ TMSCs could be passaged over 30 times when cultured as monolayer cells.

(F-G) The *in vitro* anchorage-independent growth assay. (F) Spontaneous formed spheres consisting of *NRF2*$^{AG/AG}$ TMSCs grew significantly slower than *NRF2*$^{+/+}$ TMSCs on low-attached plates. Scale bar, 1 mm. Diameter data were shown as the average value of horizontal and vertical diameters which were measured by ImageJ. The value of *NRF2*$^{+/+}$ group at day 1 was normalized to 1. Data were presented as mean ± SEM, n=10. (G) Colonies formed from *NRF2*$^{AG/AG}$ TMSCs in soft agarose were much smaller and fewer compared with the WT group. Scale bar, 50 μm. Relative colony size data were presented as mean ± SD, n >100 colonies, ***P < 0.001.

(H) Representative fluorescence images of *NRF2*$^{+/+}$ and *NRF2*$^{AG/AG}$ TMSC-injected legs 10 weeks after implantation. *NRF2*$^{+/+}$ TMSCs gave rise to sarcomas-like tumors that exhibited no boundary between tumor and surrounding muscle tissue. In sharp contrast, legs implanted with *NRF2*$^{AG/AG}$ TMSCs exhibited normal muscle-fiber patterns and no human cells were detected. Human cells were identified by GFP, muscle fibers were visualized by Laminin staining. Scale bar, 50 μm.

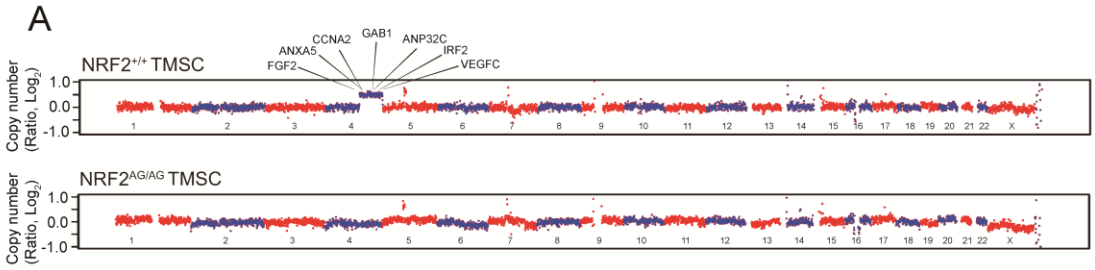
A
NRF2+/+ TMSC
CCNA2
GAB1
ANP32C
ANXA5
IRF2
FGF2
VEGFC
Copy number (Ratio, Log2)
1.0
0.0
-1.0
1 2 3 4 5 6 7 8 9 10 11 12 13 14 15 16 17 18 19 20 21 22 X
NRF2AG/AG TMSC
Copy number (Ratio, Log2)
1.0
0.0
-1.0
1 2 3 4 5 6 7 8 9 10 11 12 13 14 15 16 17 18 19 20 21 22 X

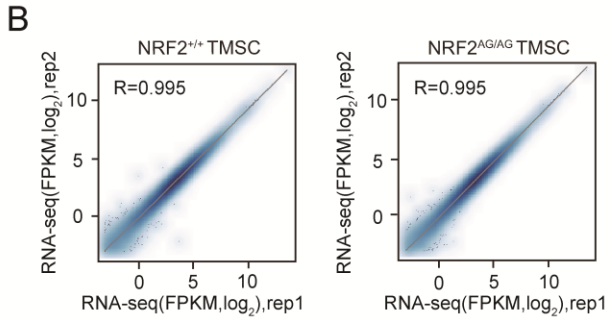
B
NRF2+/+ TMSC
R=0.995
RNA-seq(FPKM,log2),rep2
10
5
0
0 5 10
RNA-seq(FPKM,log2),rep1
NRF2AG/AG TMSC
R=0.995
RNA-seq(FPKM,log2),rep2
10
5
0
0 5 10
RNA-seq(FPKM,log2),rep1

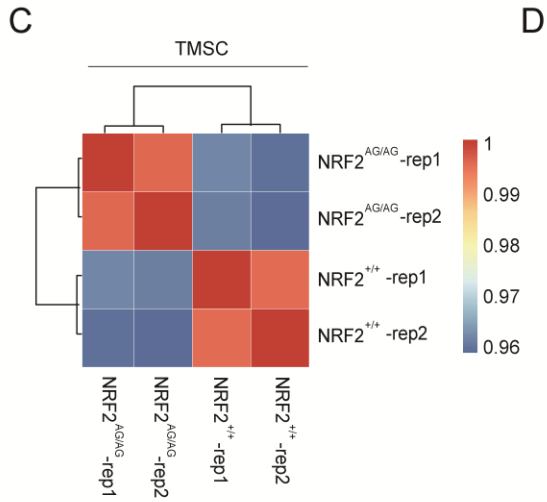
C
TMSC
NRF2AG/AG -rep1
NRF2AG/AG -rep2
NRF2+/+ -rep1
NRF2+/+ -rep2
1
0.99
0.98
0.97
0.96
NRF2AG/AG -rep1
NRF2AG/AG -rep2
NRF2+/+ -rep1
NRF2+/+ -rep2

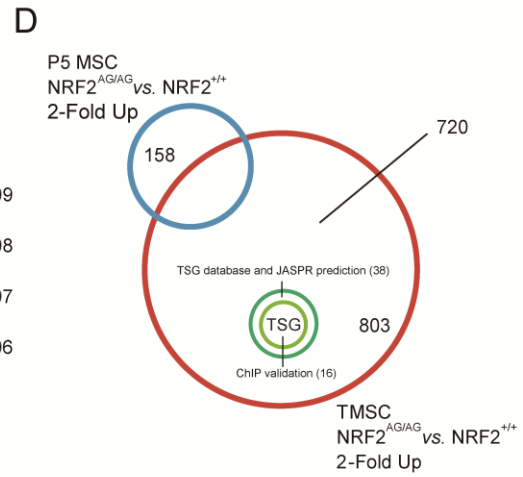
D
P5 MSC
NRF2AG/AG vs. NRF2+/+
2-Fold Up
158
720
TSG database and JASPR prediction (38)
TSG
803
ChIP validation (16)
TMSC
NRF2AG/AG vs. NRF2+/+
2-Fold Up

Supplementary information, Figure S12. Genomic and transcriptomic differences between *NRF2*$^{+/+}$ and *NRF2*$^{AG/AG}$ TMSCs

(A) Whole genome analysis of copy number variations (CNVs) in *NRF2*$^{+/+}$ and *NRF2*$^{AG/AG}$ TMSCs at P13 by deep sequencing. Tumor-promoting genes in the gain region of chromosome 4 were indicated.

(B) Scatter plots showing the correlation of gene expression (FPKM > 0.1) between duplicates of *NRF2*$^{+/+}$ and *NRF2*$^{AG/AG}$ TMSCs, respectively. The Spearman correlation coefficient was shown at the left upper side of each panel.

(C) Heatmap showing correlation of gene expression between 4 TMSC samples.

(D) Venn diagram showing that 158 genes were upregulated in P5 MSCs and 803 genes were upregulated in TMSCs after NRF2 gene editing. Among the 720 genes induced by constitutively activated NRF2 specifically in TMSCs, 38 of them were tumor suppressor genes (TSGs) containing predicted NRF2 binding sites and 16 of 38 genes were identified as NRF2-responsive TSGs in TMSCs by ChIP-qPCR.

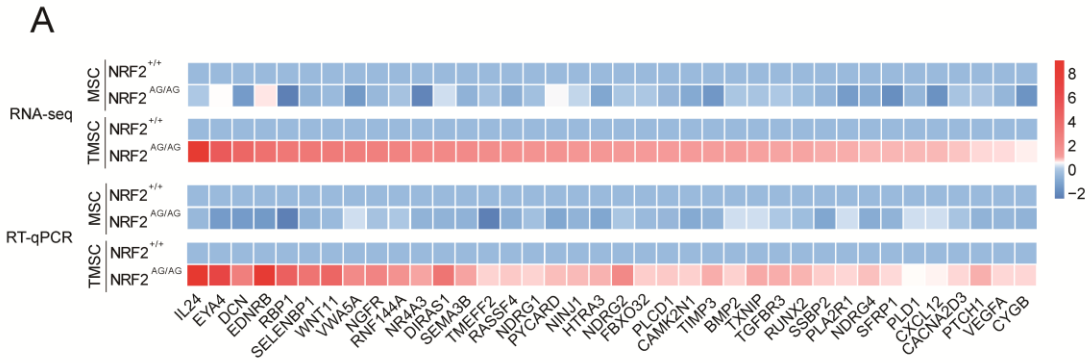

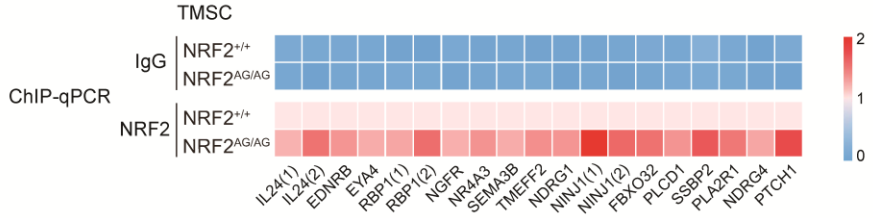

C

IL24(1)	-2308	TGCTGGCTCAT ACGACCGAGTA	-2298	NR4A3	-2848	CTGAGTGGGCA GACTCACCCGT	-2838	PLCD1	-1749	CTGAGTCAGCA GACTCAGTCGT	-1739
IL24(2)	-2619	TGCTCTGTCAC ACGAGACAGTG	-2609	SEMA3B	-3371	GTGACAAAGCA CACTGTTTCGT	-3361	SSBP2	-844	ATGAATAGGCA TACTTATCCGT	-834
EDNRB	9248	ATGAGTAAGCC TACTCATTCGG	9258	TMEFF2	-4711	ATGACTGAGCC TACTGACTCGG	-4701	PLA2R1	-2915	GGCTGTGTCAC CACTGTGTCGG	-2905
EYA4	-4943	ATGAGTTGGCA TACTCAACCGT	-4933	NDRG1	-5816	AGCTGAGTCAC TCGACTCAGTG	-5806	NDRG4	-2357	TGCTGACTCAG ACGACTGAGTC	-2347
RBP1(1)	-1911	GTGATTCAGCA CACTAAGTCGT	-1901	NINJ1(1)	-905	GTGAGTGGGCA CACTCACCCGT	-895	PTCH1	-1130	ATGACTCTGCT TACTGAGACGA	-1120
RBP1(2)	-3914	ATGAGACTGCA TACTCTGACGT	-3904	NINJ1(2)	-1959	ATGACGGAGCA TACTGCCTCGT	-1949				
NGFR	-3914	ATGACACGGCC TACTGTGCCGG	-3904	FBXO32	-2342	TGCTGTGTAAC ACGACACATTG	-2332				

Supplementary information, Figure S13. Identification of putative NRF2-responsive TSGs in TMSCs

(A) RNA-seq and RT-qPCR heatmap showing upregulation of 38 predicted NRF2-responsive TSGs in TMSCs (*NRF2*$^{AG/AG}$ vs. *NRF2*$^{+/+}$), not in hMSCs (*NRF2*$^{AG/AG}$ vs. *NRF2*$^{+/+}$). All FPKMs and RT-qPCR values of the indicated genes were normalized by the ones in *NRF2*$^{+/+}$ group and the relative expression level were presented as Log_2 (Ratio).

(B) Heatmap of ChIP-qPCR showing 16/38 putative TSGs containing NRF2 binding motifs in TMSCs. Enrichment values were normalized to input and presented as the ratio relative to NRF2 antibody-incubated *NRF2*$^{+/+}$ group.

(C) The identified NRF2 binding sites (nTGAnnnnGCn) and their relative distance from transcription start site (TSS) of the 16 putative NRF2-responsive TSGs.

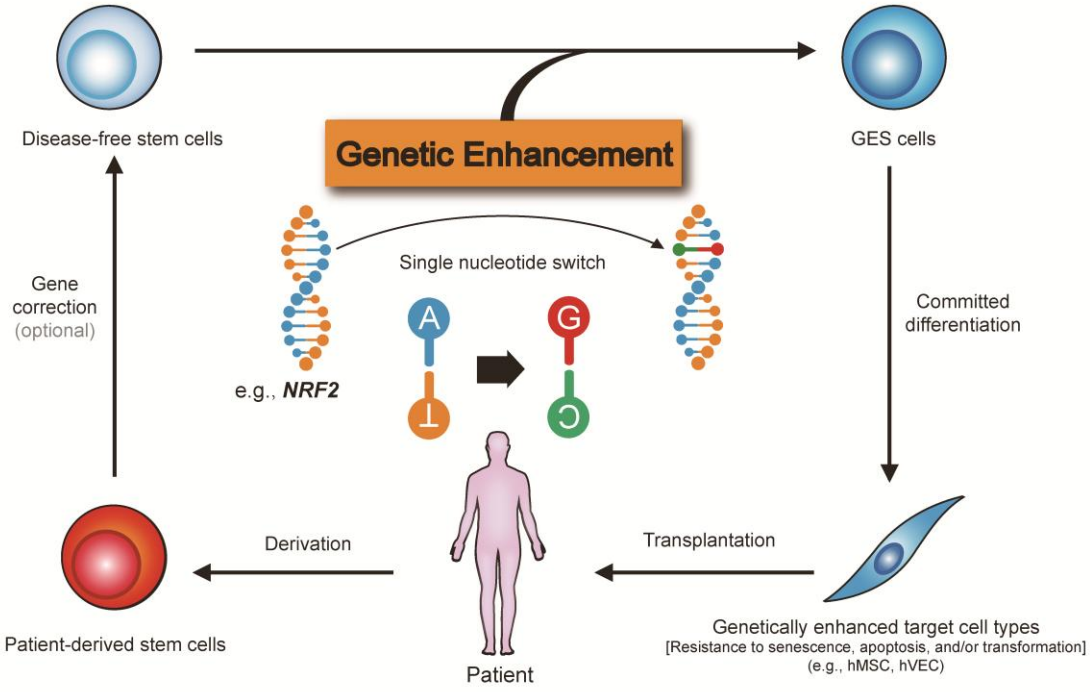
Disease-free stem cells
Genetic Enhancement
GES cells
Single nucleotide switch
A
G
e.g., NRF2
Gene
correction
(optional)
Committed
differentiation
Derivation
Transplantation
Patient-derived stem cells
Patient
Genetically enhanced target cell types
[Resistance to senescence, apoptosis, and/or transformation]
(e.g., hMSC, hVEC)

Supplementary information, Figure S14. Schematic diagram showing the application of genetic enhancement to generate superior and safer materials for cell replacement therapy

Patient-derived stem cells (with optional gene correction if the pathogenic mutation is known) could be subjected to a genetic enhancement procedure. For instance, replacement of a single nucleotide in *NRF2* gene locus via targeted gene editing to genetically enhance endogenous NRF2 pathway. The generated genetically enhanced stem (GES) cells could be differentiated to high quality target cell types with more robust generative capacity and reduced tendency to tumorigenesis for cell replacement therapy.